JOM, Vol. 67, No. 2, 2015
DOI: 10.1007/s11837-014-1210-x

Structure Analysis and Fluorescence of Mg-Al-Tb Ternary Layered Double Hydroxides and Their Calcined Products

JUNFEI CHEN,[1] ZHIGAO LEI,[1] ANQI WANG,[1] JIE LIU,[1] XIULING WU,[1,2] TIANCI CHANG,[1] YANG ZHANG,[1] and MUQING LI[1]

1.—Faculty of Materials Science and Chemistry, Engineering Research Center of Nano-Geo Materials of Ministry of Education, China University of Geosciences, Wuhan 430074, P.R. China. 2.—e-mail: xlwu@cug.edu.cn

Layered double hydroxides (LDHs) doped with Tb^{3+} ions in the brucite-like layers were prepared successfully by the co-precipitation method. The structure and fluorescence properties of Mg-Al-Tb ternary LDHs and their products calcined at different temperatures were studied for the first time. X-ray diffraction patterns indicated that as-synthesized LDH samples maintained a hexagonal crystal structure, and $Tb(OH)_3$ was detected as Tb^{3+} dopant content increasing to 5 at.%. In the fluorescent spectra, the green emission intensity arising from $^5D_4 \rightarrow {}^7F_5$ transition became stronger with the increasing ratio of Tb^{3+} dopant. When the annealing temperature rose above 500°C, the layer structure collapsed and phases of MgO and $MgAl_2O_4$ formed. Meanwhile, compared with MgAlTb-LDHs, the Tb-doped calcined LDHs (CLDHs) showed stronger luminescent intensity of $^5D_4 \rightarrow {}^7F_5$ transition. These results revealed that the calcined Mg-Al-Tb ternary LDHs may become a series of novel materials with potential applications in fluorescent devices.

INTRODUCTION

Layered double hydroxide (LDH) is a large mineral material group with a layered structure.[1] The structure of LDHs is based on hydrotalcite $Mg_6Al_2(OH)_{16}CO_3{\cdot}4H_2O$,[2] which is similar to brucite $Mg(OH)_2$.[3] In the brucite lattice, magnesium ions are surrounded octahedrally by hydroxide ions, and the octahedral units altogether form the infinite plane of two-dimensional layers. Because LDHs are derived by isomorphous substitution of Mg^{2+} cations in brucite with Al^{3+} cations, the layers bear a positive charge. Because of the increase of the anions and water molecules in the interlayer space, the whole material is still charge neutral. However, because of the great number of possible substitutes for cations and interlayer anions, the relative proportion between divalent and trivalent cations is bound to differ, thus forming a great variety of LDHs. The general formula for LDH can be represented as $[M^{2+}_{1-x}M^{3+}_x(OH)_2][A^{n-}]_{x/n}{\cdot}mH_2O$, where M^{2+} and M^{3+} are divalent and trivalent metal ions, respectively, and x is the molar ratio $M^{3+}/(M^{2+}+M^{3+})$. According to this formula, pure phases only exist for $0.2 \le x \le 0.33$.[4] M^{2+} and M^{3+} ions with ionic radius close to that of Mg^{2+} are accommodated in the brucite-like layers consisting of edge-sharing octahedral units. Therefore, M^{2+} ions can be Mg^{2+}, Zn^{2+}, Ni^{2+}, Co^{2+}, Cu^{2+}, and Ca^{2+}, whereas M^{3+} ions are usually Al^{3+}, Fe^{3+}, Cr^{3+}, and Ga^{3+}. The charge-compensating anion A^{n-} represents n-valence inorganic,[5] organic,[6] complex,[7] heteropolyacid,[8] polymer,[9] or even biochemistry[10] anions. Because LDHs have a well-defined layered structure and important functional groups, they are often identified as important in applications including anion exchangers,[11] catalysts,[12] adsorbents,[13] medical drugs,[14] and functional materials.[15,16]

Nowadays, rare-earth (RE) doped materials have been widely studied. They are attractive to researchers because they possess characteristic narrow emission bands from electronic transitions between the 4*f* energy levels and potential high efficiency, in other words, high luminous intensity and long luminous lifetime. Nevertheless, practical applications of pure RE compounds are limited because of their disadvantages such as fluorescent quenching effects and poor thermal stability. Previous studies of the luminescence properties of LDHs are often based on the intercalation of RE

(Published online November 22, 2014)

anionic complexes into the interlayer region.[17,18] However, this method may prevent other guest species from entering the interlayer region. Therefore, incorporating RE ions directly into the brucite-like lamellae without filling the interlayer area represents a great progress for the development of new fluorescent materials and a wide use of these materials in biomedical applications. Among all RE ions, trivalent terbium ions (Tb^{3+}) that produce green emissions are well-known dopants for many compounds.[19,20] For the application of fluorescent probes in biology or medical diagnosis, Tb^{3+} ion-doped layers are the most favorable. The terbium ion is a trivalent cation, with a larger ionic radius (0.0923 nm) and larger coordination number (like most lanthanide ions from 7 to 10) than the Al^{3+} ion (0.0535 nm, coordination number 6). Therefore, aimed at minimizing the lattice distortion, incorporating a small amount of Tb^{3+} ions into the hydroxide brucitic layers might be one of the prospective options.

Herein, the structure and fluorescence of Mg-Al-Tb ternary LDHs and their calcined products have been reported. It was found that LDHs have characteristic green emissions resulting from the transition $^5D_4 \rightarrow {}^7F_J$ (J = 6, 5, 4, 3) of Tb^{3+} ions.[21] Furthermore, the calcined samples exhibit much higher emission intensity than the uncalcined counterparts, which will enhance our understanding of the emissions of Tb^{3+} ions in this classic layered material and its calcined products.

EXPERIMENTAL

Materials

All the reagents were of analytical grade and used without further purification. Magnesium nitrate hexahydrate ($Mg(NO_3)_2{\cdot}6H_2O$), aluminum nitrate nonahydrate ($Al(NO_3)_3{\cdot}9H_2O$), sodium hydroxide (NaOH), and sodium carbonate anhydrous (Na_2CO_3) were purchased from Sinopharm Chemical Reagent Co., Ltd., Shanghai, China. Terbium(III) nitrate hexahydrate ($Tb(NO_3)_3{\cdot}6H_2O$) was received from Jinan Henghua Sci. & Tec. Co. Ltd., Jinan, China. Deionized water was used throughout all processes.

Materials Preparation

The co-precipitation method was used for the synthesis of LDHs samples. Fifty milliliters of an aqueous solution containing $Mg(NO_3)_2{\cdot}6H_2O$ (2 equiv., 0.050 mol, 12.82 g) and $Al(NO_3)_3{\cdot}9H_2O$ (1 equiv., 0.025 mol, 9.38 g) was dropwise added into the 50-mL aqueous solution of NaOH (7.00 g) and Na_2CO_3 (5.00 g) under vigorous stirring and reflux condensation at 70°C (approximately 3 h). The resulting white precipitate was aged at 60°C for 18 h. After that, the precipitate was filtered, washed with deionized water, and dried at 120°C for 18 h. Finally, the MgAl-CO_3-LDH powder sample was obtained after grinding. MgAlTb-CO_3-LDHs with $Mg^{2+}/(Al^{3+}+Tb^{3+})$ molar ratio of ~2 and $Tb^{3+}/(Al^{3+}+Tb^{3+})$ molar ratio of 1%, 3%, 5%, and 7% were obtained by the same method. A set of as-prepared MgAlTb-CO_3-LDHs samples were annealed in air at 500°C, 600°C, 700°C, 800°C, 900°C, and 1000°C for 5 h, respectively.

Characterization

X-ray powder diffraction (XRD) patterns of MgAlTb-CO_3-LDHs and their calcined samples were recorded on a D8-Focus diffractometer (Bruker Co., Billerica, MA) equipped with Ni-filtered and Cu Kα radiation (λ = 0.15406 nm) and operated at 40 kV and 40 mA. The diffraction peaks were for the 2θ value range 9° to 65° with a 2θ step of 0.016°. The Fourier transform infrared (FTIR) spectra were scanned over the wave number from 400 cm^{-1} to 4000 cm^{-1} using a Nicolet 6700 IR spectrometer (Thermo Fisher Scientific Inc., Waltham, MA), KBr disks. Thermogravimetric (TG) analyses and differential scanning calorimetry (DSC) were performed with a STA 409 PC thermal analyzer (NETZSCH group, Selb, Bavaria, Germany) in air flow and with a heating rate of 10°C/min. The fluorescence of the samples was studied at room temperature with the F-4500 FL spectrophotometer (Hitachi High-Tech Ltd., Tokyo, Japan). The surface morphologies were taken on a JEOL JSM-5610LV (JEOL Ltd., Tokyo, Japan) scanning electron microscope (SEM).

RESULTS AND DISCUSSION

As presented in Fig. 1, the characteristic peaks at about 11.5°, 23.3°, and 34.5° match well with LDHs XRD reflections of (003), (006), and (009), respectively (JCPDS card No: 89-0460), indicating the as-grown samples share a LDH structure with hexagonal crystal system assuming a 3R packing of layers.[22] The typical doublet of (110) and (113) planes of LDH can be observed between 60° and 63° as well. It can be found that the XRD patterns of the samples with different Al/Tb molar ratios are similar. The position of maximum peak shifts slightly to smaller 2θ degree when increasing Tb^{3+} loading from 0% to 3%. The lattice parameters were summarized in Table I.

They are given as $a = 2d_{110}$ and $c = 3(d_{003} + 2d_{006})/2$, respectively.[23] Such variation is attributed to the incorporation of Tb^{3+} into the layers of hydrotalcite structure, with a radius (0.0923 nm) larger than that of Mg and Al cations (0.072 nm and 0.0535 nm). The discrepancy of the cation radius between Tb^{3+} and Al^{3+} could induce a distortion of the layers within each octahedron, making the cation–oxygen distances no longer equal. Moreover, the cation–cation distances are only compatible with a corrugation of the octahedral layers, which lose their planarity. Hence, the conclusion that Tb^{3+} has isomorphously substituted Al^{3+} in the LDH layers can be drawn.

It is noted that when the Tb addition reaches over 3%, the secondary phase $Tb(OH)_3$ can be observed, denoting that certain Tb^{3+} cations were not incorporated in the structure (Fig. 1). The value of

parameter c decreased from 2.29382 nm to 2.29059 nm, as the provocation for the increase of strong interaction of CO_3^{2-} with the materials.[24] The diminution of parameter a has also been reported as an evidence of the effective incorporation of Tb^{3+} into the LDH framework.[25]

In Fig. 2, the FTIR spectra of the MgAl-CO_3-LDH and Tb-doped LDH samples resembled those of other hydrotalcite phases.[26,27] The strong and broad absorbance band around 3455 cm^{-1}, which is associated with the stretching vibration of hydrogen-bonded hydroxyl groups from both the LDH layers and interlayer water molecules,[10,22] is typical for these spectra. The weak band at about 1640 cm^{-1} can be ascribed to O-H bending deformations.[22,26] Three IR active absorption bands arose from the carbonate anion located at 1370 cm^{-1}(v_3), 865 cm^{-1}(v_2), and 671 cm^{-1}(v_1).[28] The evolution of the peak at about 1490 cm^{-1} with increasing Tb^{3+} loading may be attributed to a Tb-CO_3 v_3 symmetric stretching vibration. The growing intensity of this band with the increase of Tb^{3+} loading suggests the increased presence of Tb^{3+} on the hydroxide layers interacting with interlayer CO_3^{2-} species.[28] A series of bands present in the low-frequency area of the spectrum at 449 cm^{-1}, 555 cm^{-1}, 783 cm^{-1}, and 941 cm^{-1} belong to $[AlO_6]^{3-}$ condensed groups, Mg/Al-OH translation, Al-OH translation, and Al-OH deformation, respectively.[29]

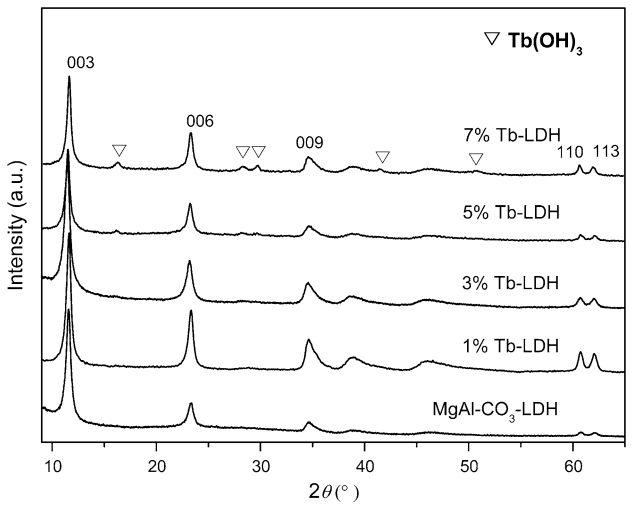

Fig. 1. X-ray diffraction patterns of LDH samples with varying levels of Tb incorporation.

Figure 3 shows the fluorescence emission spectra (λ_{ex} = 238 nm) of the samples with different Tb^{3+} content and the excitation spectrum (λ_{em} = 543 nm) of 7% Tb-LDH. The emission spectrum can be assigned to the characteristic peaks arising from the transition between $^5D_4$ level and ^7F_J (J = 6, 5, 4, 3) level of Tb^{3+}. A green luminescence can be observed under an ultraviolet lamp because $^5D_4 \rightarrow {}^7F_J$ emissions mainly fall in the green region. The corresponding emission spectra of the samples with Tb^{3+} incorporation show narrow emissions that arise from $4f \rightarrow 4f$ transitions of Tb^{3+} ions as shown in Fig. 3a.[30,31] Among the emission bands, the most remarkable green-emitting transition is $^5D_4 \rightarrow {}^7F_5$, which has been more intensive due to the nature of the dopant Tb cations in the layer. With Tb^{3+} loading increasing, an increase of the Tb^{3+} emission band at 543 nm is obvious. The other three peaks of the Tb-doped LDHs appeared at about 491 nm ($^5D_4 \rightarrow {}^7F_6$), 584 nm ($^5D_4 \rightarrow {}^7F_4$), and 620 nm ($^5D_4 \rightarrow {}^7F_3$), respectively. The emission spectrum dominated by the electric-dipole transitions indicates that the Tb cations experience a low symmetry crystal field in the materials, supporting the conclusion that the terbium ions have been included in the LDH lamellae.[32]

The 7% Tb-LDH is taken as an example for the thermal stability analysis (in Fig. 4). It is found to be similar to that of the typical weight loss process of the sample that has been reported beforehand.[33,34] Three general regions of weight loss can be easily observed coincided with one broad and two sharp endothermic peaks in the DSC profiles. The first mass loss, which is about 10.59 wt.% from room temperature to 240°C, is most likely due to the loss of interlayer water molecules in the LDH sample, together with relatively smaller amounts of carbon dioxide and water molecules resulting from the physical adsorption of the OH^- group. There are two corresponding endothermic peaks at 117.9°C and 204.7°C, respectively. It has to be noted that in a conventional LDH, the interlayer water molecules interact directly with interlayer anions and with metal cations through hydrogen bond with hydroxyl groups of the hydrotalcite lamellas; thus, the dehydration process is mainly determined by the nature of both the interlayer anions and the layer cations.[32] The second distinct mass loss of 19.88 wt.% occurs

Table I. Lattice Parameters for the LDH Samples

Samples	d_{003} (nm)	d_{006} (nm)	d_{110} (nm)	a (nm)	c (nm)
MgAl-CO_3-LDH	0.76413	0.38042	0.15198	0.30396	2.28746
1% Tb-LDH	0.76517	0.38186	0.15245	0.30490	2.29334
3% Tb-LDH	0.76533	0.38194	0.15247	0.30494	2.29382
5% Tb-LDH	0.76495	0.38188	0.15239	0.30478	2.29307
7% Tb-LDH	0.76384	0.38161	0.15235	0.30470	2.29059

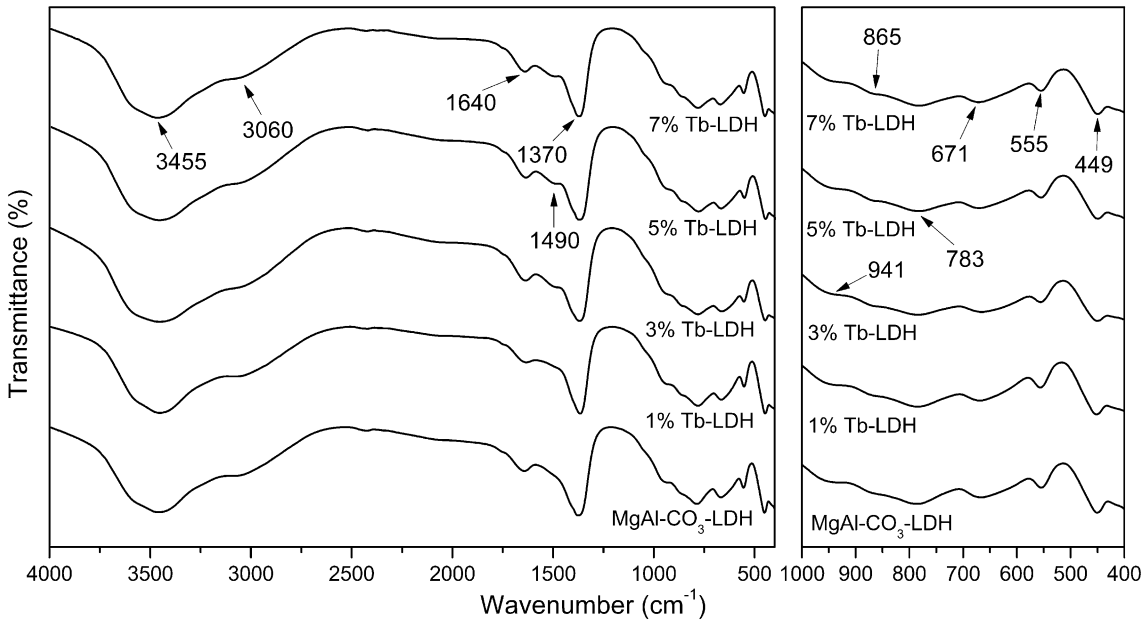

Fig. 2. FTIR spectra of LDH samples with increased Tb loading (left) 4000–400 cm^{-1} and (right) 1000–400 cm^{-1}.

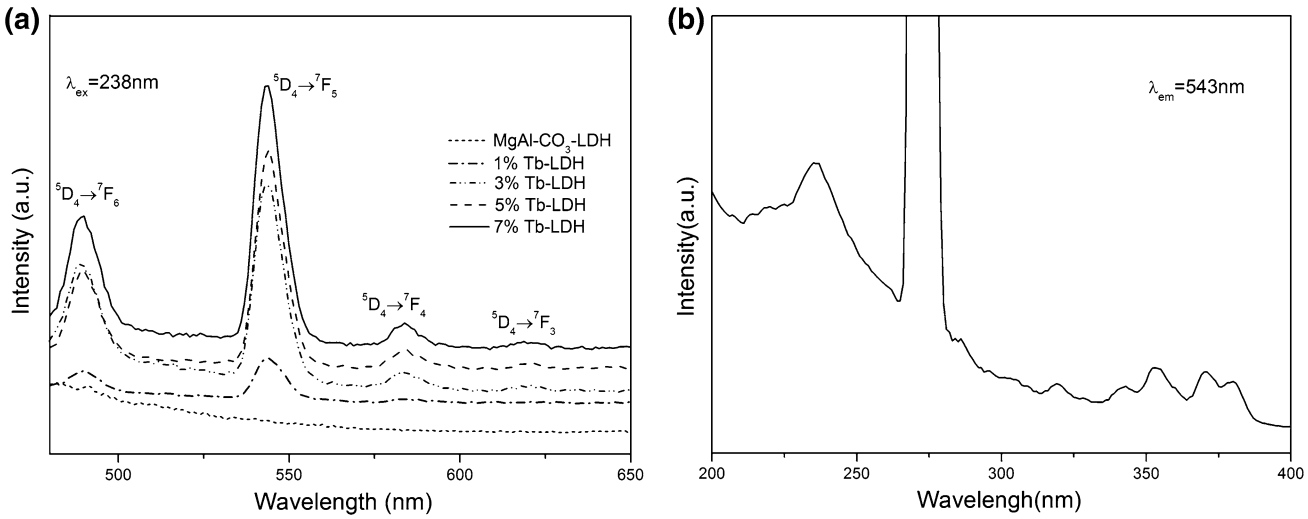

Fig. 3. (a) Fluorescence emission spectra (λ_{ex} = 238 nm) of LDH samples with different Tb loading and (b) excitation spectrum (λ_{em} = 543 nm) of 7% Tb doped LDH.

in the temperature range of 240°C to 400°C, which is ascribed to the removal of hydroxyl groups from the hydrotalcite-like layers, corresponding to the remarkable sharp DSC endothermic peak centered at 353.8°C. The third stage of weight loss above 400°C should be attributed to the decomposition of residual hydroxyl groups and the CO_3^{2-} from the interlayer space.[35] Then, the TG curve turns smooth with the temperature increasing to 500°C, indicating the completely decomposed sample. The layer structure has collapsed and the solid solution of relevant metal oxides is formed at the same time.[36]

Thermal calcination of LDH often produces very reactive mixed oxides, commonly called calcined layered double hydroxides (CLDHs). A general view in Fig. 5 demonstrates the XRD patterns of 7% Tb^{3+} loading LDHs heated from 500°C to 1000°C. Tb-doped CLDH obtained at 500°C results in an almost complete decomposition of the CO_3^{2-} from the interlayer space, evolving to CO_2 and water. Consequently, a main magnesium oxide phase is formed. The major reflections of MgO are broadened owing to the poor crystallinity of the sample. Some Al^{3+} ions in the structure are dissolved in the lattice of MgO, resulting in the formation of a mixed solid solution that is capable of being restored to a LDH when rehydrated.[37] When the calcination temperature increased to 800°C, no major changes

happened. The sharpness of the peaks increases with the calcination temperature, which is in line with the outcome of progressive crystal growth of MgO and $Tb_4Al_2O_9$ phases due to sintering of the sample. At calcination temperatures of 800°C and above, new peaks attributed to the formation of $MgAl_2O_4$ spinel appear with a lower intensity. These maximum diffraction peaks are much weaker than those of the MgO phase, revealing a lower crystallinity and smaller amount of the $MgAl_2O_4$ phase. The Al^{3+} ions, which have smaller ionic radius than Mg^{2+} ions, are progressively released from the MgO-like structure to spinel $MgAl_2O_4$ and $Tb_4Al_2O_9$ phase.[38,39] According to Scherrer equation, crystallite sizes of 7% Tb-doped CLDHs are calculated in Table II. Crystal grows along with the increased temperature.

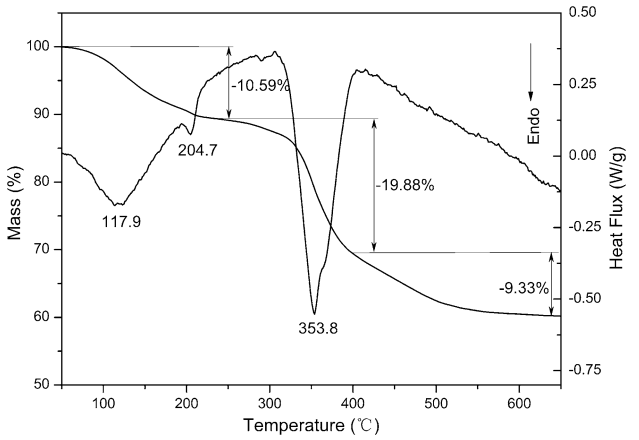

Fig. 4. TG and DSC curves of 7% Tb^{3+} doped MgAlTb-CO_3-LDH. Operative condition: air flow, heating rate 10°C/min

The emission intensity of Tb-doped CLDHs varies as the annealing temperature increases from 500°C to 1000°C. Figure 6 displays the emission spectra of 7% Tb^{3+} loading CLDHs calcined at different temperatures (λ_{ex} = 238 nm). Compared with the Tb-doped LDHs, peaks of annealed samples have almost no shift, and the strongest peak still shows up at 543 nm with the dominant electric-dipole transition $^5D_4 \rightarrow {}^7F_5$. All the annealed samples have much stronger peaks than uncalcined LDHs. The insert of Fig. 6 represents the intensity trend of $^5D_4 \rightarrow {}^7F_5$ peaks at different temperatures. The intensity of the transition $^5D_4 \rightarrow {}^7F_5$ increases with the calcination temperature and reaches a plateau at 800°C. Combined with the XRD patterns in Fig. 5, the crystal structure of 7% Tb^{3+} loading

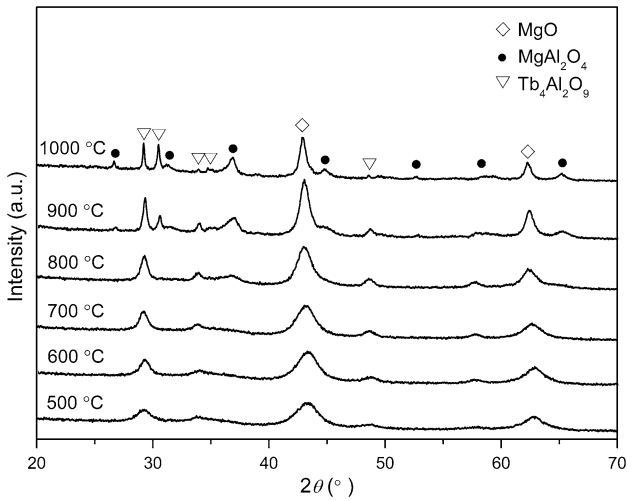

Fig. 5. XRD patterns of calcined 7% Tb-LDH samples at various temperatures

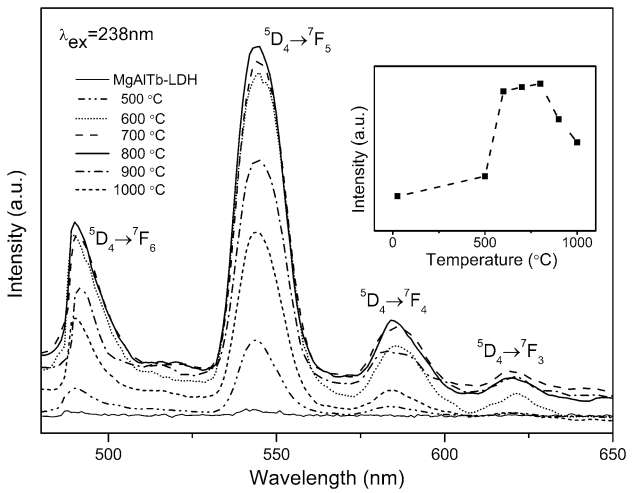

Fig. 6. Fluorescence emission spectra of 7% Tb-CLDH samples with different annealing temperatures

Table II. Crystallite sizes of 7% Tb-doped CLDHs at different temperatures

Temperature (°C)	2θ (°)	FWHM	Crystallite size (nm)
500	43.2949	1.8380	4.5984
600	43.2149	1.6580	5.0963
700	43.1051	1.5580	5.4213
800	43.0052	1.3290	6.3533
900	42.9752	0.8290	10.1841
1000	42.8975	0.5990	14.0907

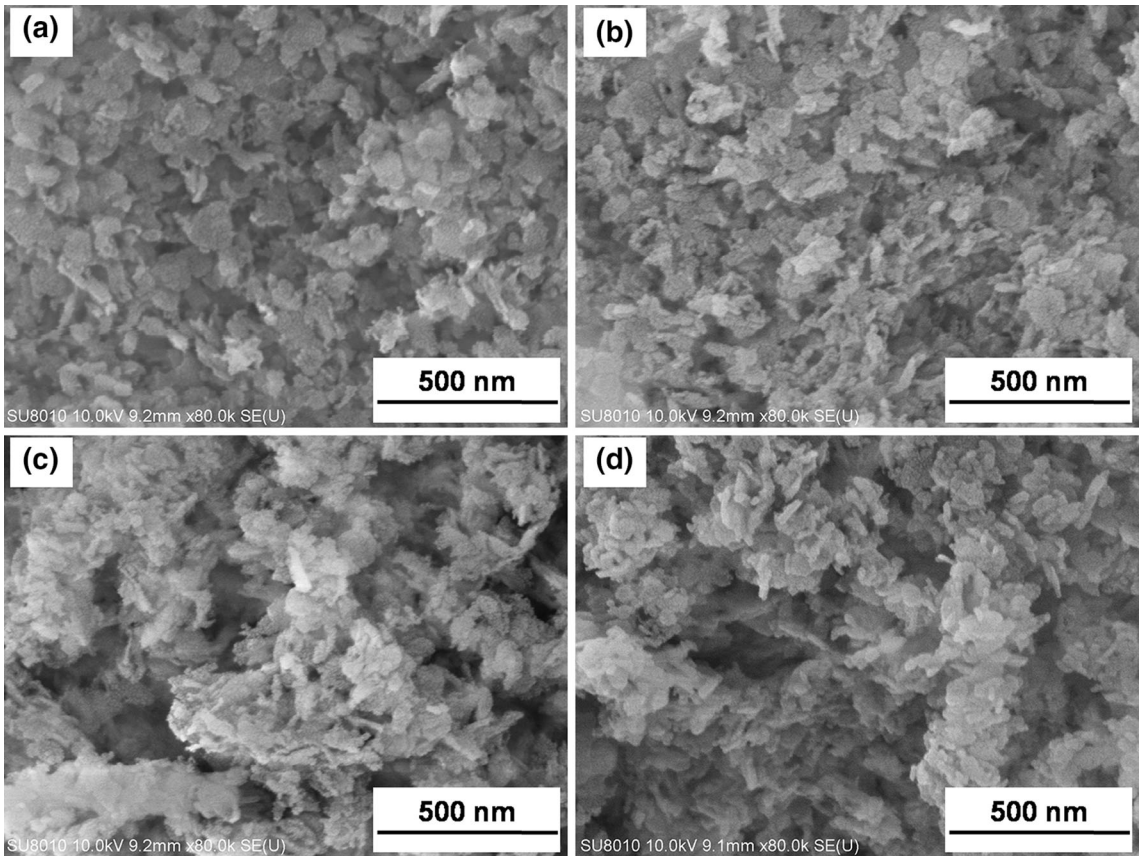

Fig. 7. SEM micrographs of 7% Tb-CLDHs annealed at (a) 700°C, (b) 800°C, (c) 900°C, and (d) 1000°C.

CLDH calcined at 800°C is more complete than the solid solution at 500–700°C. The result suggests that, to some extent, more complete structure and larger crystallite size are in favor of crystal fluorescence. When the temperature goes higher than 800°C, the emission of transition $^5D_4 \rightarrow {}^7F_5$ is greatly weakened. This is attributed to the high calcined temperature but not to the formation of a new phase $MgAl_2O_4$[40] because the emissions of transition $^5D_4 \rightarrow {}^7F_J$ (J = 6, 5, 4, 3) can be observed in the Tb-doped $MgAl_2O_4$ structure.[41] Calcined temperature over 800°C will lead to the fluorescence quenching of Tb^{3+} ions. The emission intensity falls and fluorescence effect of the sample is weakened.

SEM micrographs of the annealed samples at 700°C, 800°C, 900°C and 1000°C are shown in Fig. 7 respectively. After the 7% Tb-doped sample was annealed at 700°C, the platy grains became irregular and aggregated. As temperatures increased, the grains grew larger and agglomeration was more apparent.

CONCLUSION

In summary, structure and fluorescence of the ternary LDHs and the annealed products were investigated in the research. Seven percent Tb^{3+} loading LDH has stronger emission intensity in green light-emitting area among 0–7% Tb-doped LDHs. Annealing the optimum concentration at 7% Tb-doped LDH under different temperature, the resulting CLDH annealed at 800°C gives the maximum $^5D_4 \rightarrow {}^7F_5$ luminescence intensity with a more complete structure and larger crystallite size. After the temperature rises over 800°C, emission intensity falls due to the fluorescence quenching of Tb^{3+} ions. Overall, calcined Mg-Al-Tb LDHs may become a series of novel materials with potential applications in fluorescent devices.

ACKNOWLEDGEMENTS

This work was supported by the National Natural Science Foundation of China (Nos. 41172051 and 21203170), the National College Students' Innovative Training Program (No. 201310491012), the Fundamental Research Founds for National University (No. 1410491B04), and the Teaching Laboratory Opening Funds (No. SKJ2013008 and SKJ2013020), China University of Geosciences (Wuhan).

REFERENCES

1. A.I. Khan and D. O'Hare, *J. Mater. Chem.* 12, 3191 (2002).
2. F. Cavani, F. Trifiròand, and A. Vaccari, *Catal. Today* 11, 173 (1991).

3. F. Pascale, S. Tosoni, C. Zicovich-Wilson, P. Ugliengo, R. Orlando, and R. Dovesi, *Chem. Phys. Lett.* 396, 308 (2004).
4. M.R. Weir, J. Moore, and R.A. Kydd, *Chem. Mater.* 9, 1686 (1997).
5. R. Ma, Z. Liu, K. Takada, N. Iyi, Y. Bando, and T. Sasaki, *J. Am. Chem. Soc.* 129, 5257 (2007).
6. Y. Tian, G. Wang, F. Li, and D.G. Evans, *Mater. Lett.* 61, 1662 (2007).
7. F. Malherbe and J.P. Besse, *J. Solid State Chem.* 155, 332 (2000).
8. S.K. Yun and T.J. Pinnavaia, *Inorg. Chem.* 35, 6853 (1996).
9. Z. Liu, R. Ma, M. Osada, N. Iyi, Y. Ebina, K. Takada, and T. Sasaki, *J. Am. Chem. Soc.* 128, 4872 (2006).
10. S. Aisawa, H. Kudo, T. Hoshi, S. Takahashi, H. Hirahara, Y. Umetsu, and E. Narita, *J. Solid State Chem.* 177, 3987 (2004).
11. A.V. Radha, P. Vishnu Kamath, and C. Shivakumara, *Solid State Sci.* 7, 1180 (2005).
12. M. Verónica, B. Graciela, A. Norma, and L. Miguel, *Chem. Eng. J.* 138, 602 (2008).
13. L. Ai, C. Zhang, and L. Meng, *J. Chem. Eng. Data* 56, 4217 (2011).
14. M. Wei, M. Pu, J. Guo, J. Han, F. Li, J. He, D.G. Evans, and X. Duan, *Chem. Mater.* 20, 5169 (2008).
15. R. Wen, Z. Yang, H. Chen, Y. Hu, and J. Duan, *J. Rare Earth* 30, 895 (2012).
16. A.W. Musumeci, G.M. Mortimer, M.K. Butler, Z.P. Xu, R.F. Minchin, and D.J. Martin, *Appl. Clay Sci.* 48, 271 (2010).
17. T. Posati, F. Bellezza, A. Cipiciani, F. Costantino, M. Nocchetti, L. Tarpani, and L. Latterini, *Cryst. Growth Des.* 10, 2847 (2010).
18. E. Angelescu, O.D. Pavel, R. Bîrjega, R. Zăvoianu, G. Costentin, and M. Che, *Appl. Catal. A* 308, 13 (2006).
19. J. Kido and Y. Okamoto, *Chem. Rev.* 102, 2357 (2002).
20. E.A. Raja, S. Menon, B. Dhabekar, N.S. Rawat, and T.K. Gundu Rao, *J. Lumin.* 129, 829 (2009).
21. I. Omkaram, G. Seeta Rama Raju, and S. Buddhudu, *J. Phys. Chem. Solids* 69, 2066 (2008).
22. Y. Guo, Z. Zhu, Y. Qiu, and J. Zhao, *J. Hazard. Mater.* 239, 279 (2012).
23. R. Bîrjega, O.D. Pavel, G. Costentin, M. Che, and E. Angelescu, *Appl. Catal. A* 288, 185 (2005).
24. Tzompantzi, Y. Carrera, G. Morales-Mendoza, G. Valverde-Aguilar, and A. Mantilla, *Catal. Today* 212, 164 (2013).
25. F. Tzompantzi, G. Mendoza-Damián, J.L. Rico, and A. Mantilla, *Catal. Today* 220, 56 (2014).
26. H. Chen and W.G. Zhang, *J. Am. Ceram. Soc.* 93, 2305 (2010).
27. J. Fang, M. Li, Q. Li, W. Zhang, Q. Shou, F. Liu, X. Zhang, and J. Cheng, *Electrochim. Acta* 85, 248 (2012).
28. A.W. Musumeci, Z.P. Xu, S.V. Smith, R.F. Minchin, and D.J. Martin, *J. Nanopart. Res.* 12, 111 (2010).
29. L. El Gaini, M. Lakraimi, E. Sebbar, A. Meghea, and M. Bakasse, *J. Hazard. Mater.* 161, 627 (2009).
30. S. Rodriguez-Liviano, F.J. Aparicio, T.C. Rojas, A.B. Hungría, L.E. Chinchilla, and M. Ocaña, *Cryst. Growth Des.* 12, 635 (2012).
31. S.S. Pitale, V. Kumar, I. Nagpure, O.M. Ntwaeaborwa, and H.C. Swart, *Curr. Appl. Phys.* 11, 341 (2011).
32. T. Posati, F. Costantino, L. Latterini, M. Nocchetti, M. Paolantoni, and L. Tarpani, *Inorg. Chem.* 51, 13229 (2012).
33. S. Livi, V. Bugatti, L. Estevez, J. Duchet-Rumeau, and E.P. Giannelis, *J. Colloid Interface Sci.* 388, 123 (2012).
34. I. Cota, E. Ramírez, F. Medina, J.E. Sueiras, G. Layrac, and D. Tichit, *Appl. Catal. A* 382, 272 (2010).
35. K. Rozov, U. Berner, C. Taviot-Gueho, F. Leroux, G. Renaudin, D. Kulik, and L.W. Diamond, *Cem. Concr. Res.* 40, 1248 (2010).
36. W. Yang, Y. Kim, P.K.T. Liu, M. Sahimi, and T.T. Tsotsis, *Chem. Eng. Sci.* 57, 2945 (2002).
37. S. Miyata, *Clays Clay Miner.* 28, 50 (1980).
38. F. Millange, R.I. Walton, and D. O'Hare, *J. Mater. Chem.* 10, 1713 (2000).
39. E. Kanezaki, *Solid State Ionics* 106, 279 (1998).
40. Y. Chen, S. Zhou, F. Li, J. Wei, Y. Dai, and Y. Chen, *Clay Miner.* 46, 487 (2011).
41. J. Wang, J. Ye, Y. Lin, W. Chen, and G. Ning, *J. Nanosci. Nanotechnol.* 10, 574 (2010).